

Radiative Jet Experiments of Astrophysical Interest Using Intense Lasers

D. R. Farley,¹ K. G. Estabrook,¹ S. G. Glendinning,¹ S. H. Glenzer,¹ B. A. Remington,¹ K. Shigemori,² J. M. Stone,³
R. J. Wallace,¹ G. B. Zimmerman,¹ and J. A. Harte¹

¹Lawrence Livermore National Laboratory, Livermore, California 94551

²Lawrence Livermore National Laboratory, Livermore, California 94551,
and Institute of Laser Engineering, Osaka University, Suita, Osaka, Japan

³Department of Astronomy, University of Maryland, College Park, Maryland 20742

(Received 16 March 1999)

A high Mach number, radiatively cooled jet of astrophysical interest has been produced using intense laser irradiation of a gold cone. The evolution of the jet was imaged in emission and in radiography, and the temperature was measured with Thomson scattering. Comparison with numerical simulations shows that radiative cooling is a dominant mechanism in the collapse of the Au plasma jet on axis, with temperatures plummeting and peak densities increasing, each by an order of magnitude in $\sim \frac{1}{2}$ ns. In dimensionless terms, aspects of this jet are similar to radiative astrophysical jets.

PACS numbers: 52.50.Jm, 52.65.Kj, 95.30.Qd, 98.62.Nx

High Mach number, radiatively cooled jets are observed throughout the galaxy, one example being the Herbig-Haro (HH) objects [1]. These HH jets are characterized by radiative shock fronts associated with highly collimated, high Mach number outflows from newly formed stars. Their morphology and kinematics have been modeled with numerical simulations, and the need to include radiative cooling has been emphasized [2,3]. Most astrophysical jets are supersonic, and their dynamics are sensitive to Mach number (jet speed/sound speed) [4]. Regimes exist where magnetic [5] and relativistic [6] effects are also important. Depending on the density and temperature, radiation can cool a plasma jet, allowing the jet to collapse to a smaller radius and higher density, which modifies the dynamics of the jet penetrating the interstellar medium. The implementation of radiative effects into multidimensional hydrodynamic simulations is not trivial, and comparison with experimental benchmark data would be highly beneficial. Such experiments are possible through the use of high-power lasers.

Supersonic jet experiments [7] have been previously conducted on the Nova laser [8]. The jets produced were high Mach number ($M = 10-20$), but adiabatic (nonradiative) due to their high densities ($\rho \sim 1 \text{ g/cm}^3$) and low temperatures ($T \leq 50 \text{ eV}$). In a new experiment, highly radiative jets of astrophysical interest have been produced using the Nova laser. Comparisons with numerical simulations show the strong effect of radiative cooling.

The experimental design is shown in Fig. 1. The target is a gold disk with a 120° included angle conical section machined out of one side. The interior of the conical section is illuminated simultaneously by five Nova beams, each using a 100 ps full width at half maximum (FWHM) Gaussian pulse shape at 351 nm wavelength and at an energy of approximately 225 J. The spot size of each beam was elliptical with partly overlapping dimensions of approximately $260 \mu\text{m} \times 410 \mu\text{m}$, and each beam was incident nearly perpendicular (within 10°) to the cone

surface. This resulted in an axisymmetric, uniform ring of illumination on the conical concave surface at an average intensity of $\sim 2 \times 10^{15} \text{ W/cm}^2$, causing rapid ablation of plasma normal to the surface. This hot plasma collided on axis at $t = 0.3-0.5 \text{ ns}$ after the peak of the laser pulse to produce a jet which propagated axially away from the cone. As the Au plasma collided on axis, the ion-ion mean free path length, λ_{ii} , is small compared to characteristic spatial scales such as r_0 , the radius of the jet (e.g., $\lambda_{ii} \ll r_0$). Hence, the plasma jet is collisional and can be satisfactorily modeled with a radiation-hydrodynamics code.

The diagnostics used in the experiment are shown in Fig. 1. Three gated x-ray pinhole cameras [9,10] were used to record two-dimensional, time-resolved images of the jet. Two of these cameras recorded the self-emission from the jet from side-on and face-on views. The third recorded a side-on, backlit radiograph of the jet using a uranium foil irradiated by one of Nova's remaining beams as a backlighter source. The uranium x-ray energy spectrum peaks at $\sim 1 \text{ keV}$ [11]. The two

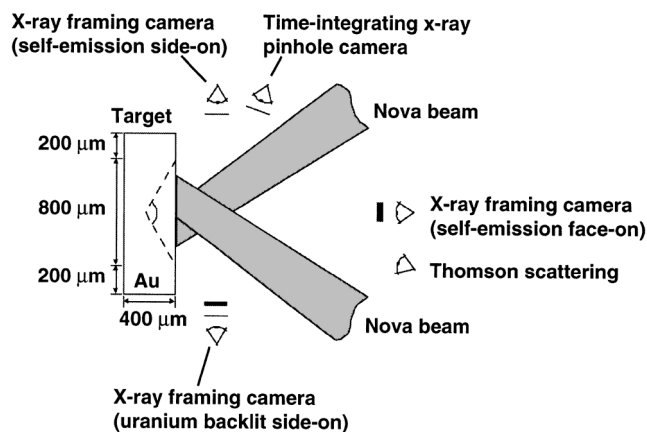


FIG. 1. Schematic of the radiative jet experiment and primary diagnostics.

side-on cameras each used thin filters of $1\ \mu\text{m}$ thick lexan ($\text{C}_{16}\text{H}_{14}\text{O}_3$; $\rho = 1.2\ \text{g}/\text{cm}^3$) substrate layered with $3000\ \text{\AA}$ of aluminum to block stray light, and the backlit camera had an additional $12.5\ \mu\text{m}$ of beryllium filtering. All the x-ray pinhole cameras used $10\ \mu\text{m}$ pinholes, and the instrument spatial resolution is therefore approximately $10\ \mu\text{m}$ [12]. A Thomson scattering diagnostic [13] was used to measure the electron temperature at a position of $300\ \mu\text{m}$ from the cone face at $0.5\text{--}0.6\ \text{ns}$ after the peak of the laser pulse.

Extensive numerical simulations were done in the development of the radiative jet experiments, using the two-dimensional radiation-hydrodynamics code LASNEX [14]. Several different experimental designs were considered, and the present configuration was chosen based on the strong radiative cooling effects predicted. In the simulations, the laser energy deposition was done by the ray-trace technique, whereby ~ 1000 laser rays were propagated up to the gold surface. For each ray, energy is absorbed by inverse bremsstrahlung along its path and by resonance absorption at the critical surface. LASNEX self-consistently calculates electron and ion temperatures and x-ray photon distributions along with the hydrodynamic plasma flow. An average atom model was used in calculating average ionization level $\langle z \rangle$. The radiation transport algorithm used in the simulations was multigroup diffusion, assuming the plasma was not in local thermodynamic equilibrium, with 256 to 512 bins encompassing photon energies from 1 to 30 keV and with detailed emission and absorption lines [15,16].

Two-dimensional images of self-emission from the jet at $1.1\ \text{ns}$ after the peak of the laser pulse from experiment and simulation are shown in Figs. 2(a) and 2(b), respectively. In the simulation, the jet was assumed to be axisymmetric, and the results qualitatively reproduce the jet morphology observed in the experimental data. Note the central region of the beam does not radiate as strongly as the outer limbs of the jet. This is due to large radiative losses in the denser central region early in time, since radiative losses vary as $q_{\text{rad}} \sim n_i^2$, where n_i is the ion density. This preferentially cools the core while the outer, lower density region remains hot and continues to radiate later in time. The LASNEX simulation qualitatively reproduces this preferential core cooling, with the temperature on axis a factor of ~ 30 lower than in the outer envelope at $1.1\ \text{ns}$. Radial profiles from the images in Figs. 2(a) and 2(b) are shown in Fig. 2(c). Each profile represents the average of a $10\ \mu\text{m}$ wide band located at approximately $950\ \mu\text{m}$ from the cone face and was normalized by its integral. This preferential core cooling manifests itself as a double peaked structure in the radial profiles, with the peaks separated by $\sim 20\ \mu\text{m}$ in the simulation, whereas the separation observed in the experiment is a factor of 3 larger at $\sim 60\ \mu\text{m}$. This discrepancy is most likely due to the azimuthal asymmetries in laser illumination in the experiment, causing tangential velocities. The simulation

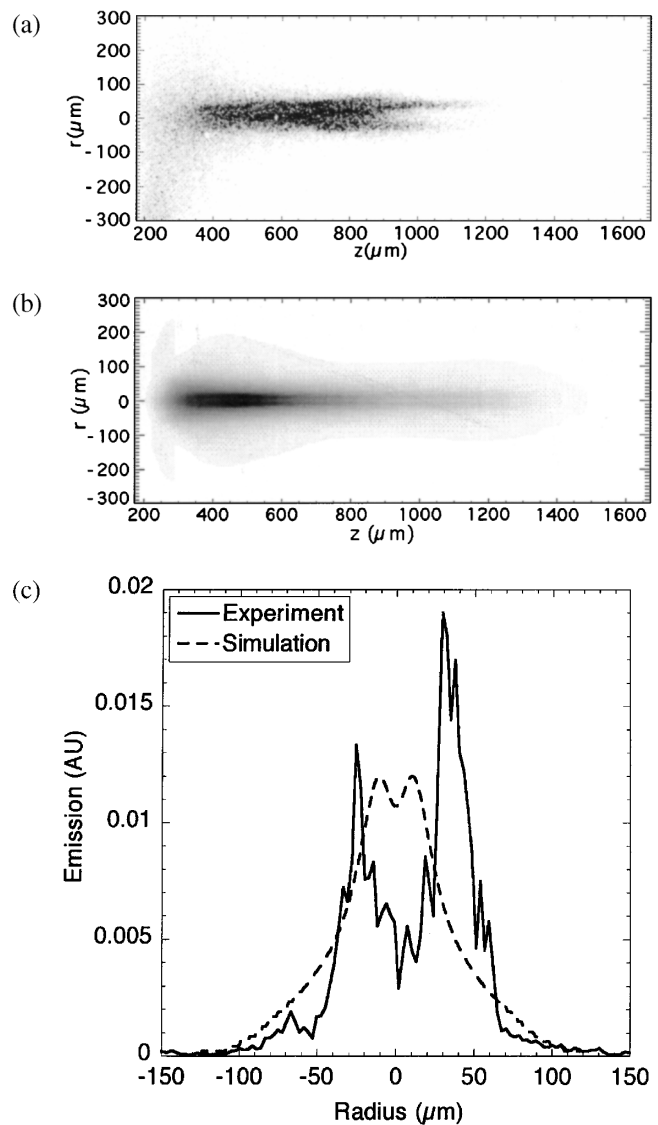


FIG. 2. Images of self-emission at $1.1\ \text{ns}$ from the radiative jet from (a) experiment; (b) LASNEX simulation; (c) emission from experiment and LASNEX simulation using the transmission distributions (averaged over $10\ \mu\text{m}$) from self-emission images at $z = 950\ \mu\text{m}$.

is azimuthally symmetric, which allows the “imploding” Au plasma to collapse down to a narrower, denser jet on axis.

The experimental and simulated backlit radiographs are shown in Figs. 3(a) and 3(b), respectively, taken at $1.3\ \text{ns}$ after the peak of the laser pulse. The simulated result has been postprocessed to include the smearing due to the finite spatial resolution of the diagnostic. The beam is well collimated along the observed length of the jet, and the simulated radiograph qualitatively reproduces the data. Radial profiles averaged over $10\ \mu\text{m}$ in the axial direction were generated from the images of Figs. 3(a) and 3(b) at a location of approximately $950\ \mu\text{m}$ from the cone face and normalized by the backlighter transmission outside of the jet region. The natural logarithm of this normalized transmission, shown in Fig. 3(c), depicts the lateral optical

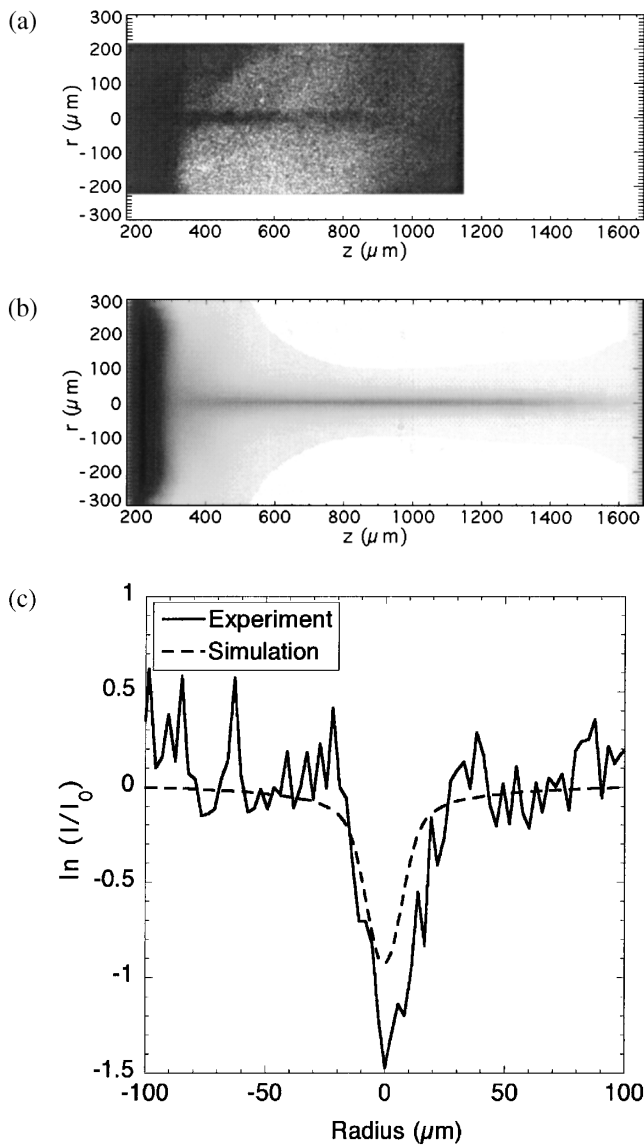


FIG. 3. Radiographs of the jet (in exposure) at 1.3 ns using uranium backlighting from (a) the experiment, (b) the LASNEX simulation, and (c) the natural log of normalized profiles from (a) and (b), each averaged over 10 μm at a location of $z = 950 \mu\text{m}$ from the face of the cone.

depth of the jet, $\delta_{\text{jet}} = 2 \int_0^{r_0} \rho \kappa dr$, where κ (cm^2/g) and r_0 correspond to opacity and outer radius of the jet, respectively. The peak optical depth from the simulation is about 60% of that measured, as is the FWHM (39 μm from the experiment versus 23 μm from the simulation). This discrepancy may be a spatial resolution effect. The azimuthally symmetric simulation predicts higher convergence of plasma than actually occurs, giving more mass located in a region below the resolution limit of the diagnostic and therefore a lower predicted optical depth. A jet radial velocity was estimated from the data to be approximately $13 \pm 3 \mu\text{m}/\text{ns}$ for times between 0.9 and 1.7 ns after the laser pulse, and a lower radial velocity at later times. An observed jet tip speed of $v_{\text{jet}} = 650 \pm 130 \mu\text{m}/\text{ns}$ was measured at times between 0.5 and

0.9 ns, which compares reasonably well with 750 $\mu\text{m}/\text{ns}$ predicted by LASNEX. The simulation suggests this jet tip speed does not change significantly with time.

The dynamics of the radiative collapse is illustrated in Figs. 4(a) and 4(b) with profiles from LASNEX simulations of density and electron temperature along the axis. As shown in Fig. 4(a), the jet density on axis increases monotonically with time, starting at 0.025 g/cm^3 at 0.3 ns, and increasing to $\sim 0.2 \text{ g}/\text{cm}^3$ at 0.8 ns. The temperature profiles shown in Fig. 4(b) change more dramatically. The temperature near the location of peak density drops precipitously from $\sim 2 \text{ keV}$ at 0.3 ns to about 75 eV at 0.8 ns, as a result of the prodigious energy removal by radiation. The simulated temperatures are confirmed by the Thomson scattering measurement [13], giving $T_e = 250 \pm 40 \text{ eV}$ at 0.5–0.6 ns, as shown by the

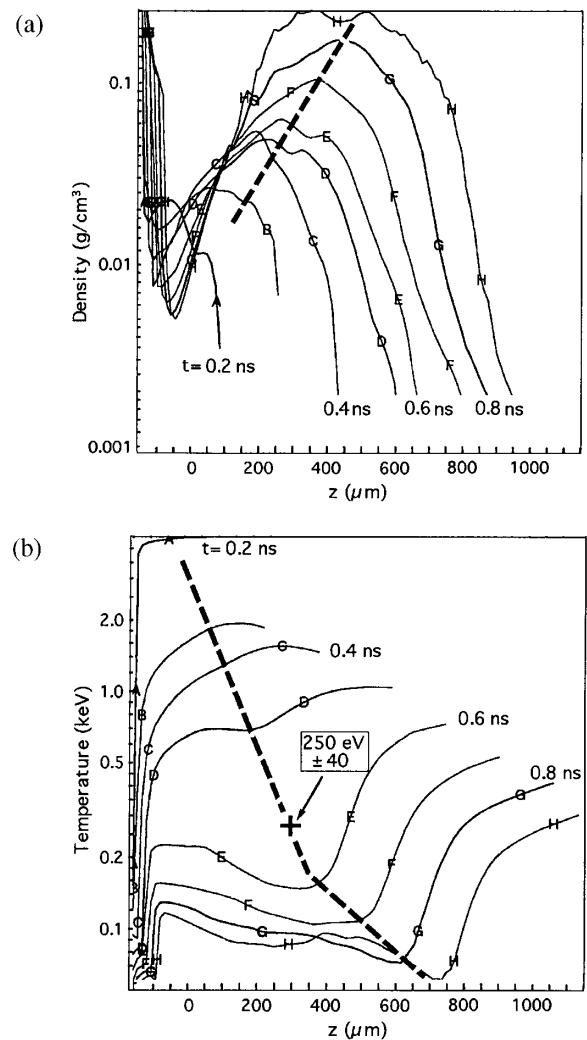


FIG. 4. Profiles of (a) density and (b) electron temperature along the jet axis in 0.1 ns increments, starting at 0.2 ns from the LASNEX simulations. The thick dashed lines are meant only to guide the eye in following the radiative collapse. The single data point in (b) corresponds to the Thomson scattering temperature measurement at 0.5–0.6 ns and a position of 300 μm from the face of the cone.

data point at $z = 300 \mu\text{m}$ in Fig. 4(b). This result falls well within the precipitous drop in temperatures predicted at 0.5–0.6 ns. The effect of radiation is observed by comparing simulations with and without radiation included. From comparison of radial profiles for the “radiation on” and “radiation off” cases, it was found that the jet density on axis is a factor of 2–100 times higher (depending on time and location) in the radiation on case than the radiation off case, as the radiative emissions cool the core of the plasma.

LASNEX output was used to determine several parameters relevant to the dynamics and characterization of the jet. As the Au plasma collides on the axis of the cone, the ion temperature (T_i) is initially higher than the electron temperature (T_e). Electron-ion collisions, however, drive the electron and ion fluids towards a common temperature with a characteristic equilibration time τ_{ei} , defined by $dT_e/dt = (T_i - T_e)/\tau_{ei}$, which can be calculated by [17] τ_{ei} (sec) = $5.6 \times 10^{18}(m_e T_i + m_i T_e)^{3/2}/(m_e m_i)^{1/2}\langle Z \rangle n_e \lambda$. Here, m_e and m_i are the electron and ion masses, respectively, $\langle Z \rangle$ is the average ionization state, and λ is the Coulomb logarithm approximated by [17] $\lambda = 23 - \ln(n_e^{1/2}\langle Z \rangle T_e^{-3/2})$. Using values from LASNEX, τ_{ei} is estimated to be 0.9 ± 0.2 ns and 0.2 ± 0.1 ns at 0.5 ns and 0.6 ns after the laser pulse, respectively, averaged over the beam diameter at $z = 300 \mu\text{m}$. This precipitous drop in τ_{ei} over 100 ps results from the $\tau_{ei} \sim T^{3/2}/(\langle Z \rangle^2 \rho)$ dependence, where T_e on axis drops by a factor of ~ 4 from 0.5 to 0.6 ns, while density increases by $\sim 30\%$, and $\langle Z \rangle$ decreases by $\sim 25\%$. Simulations show that the jet is radiatively cooled through emission of primarily 0.8–3 keV photons. Early in time ($t \approx 0.5$ ns) the jet plasma is optically thin to these photons, with a photon mean free path length of $\sim 200 \mu\text{m}$ for 1 keV x rays, compared to a jet diameter of $< 50 \mu\text{m}$. Later in time ($t \approx 0.9$ ns) the photon mean free path has dropped to $\sim 1 \mu\text{m}$, as the plasma density increases and its temperature decreases, and the plasma becomes optically thick. To estimate a characteristic radiative cooling time, τ_{rad} , an optically thin plasma was assumed and the ratio of thermal energy density to radiative flux was used, as given by $\tau_{\text{rad}} = \varepsilon_{\text{thm}}/q_{\text{rad}}$. Here, ε_{thm} (erg/cm³) = $3n_e k(T_i/\langle Z \rangle + T_e)/2$, and q_{rad} (erg/cm² s) includes photons resulting from bound-bound, bound-free, and free-free transitions. Using results from LASNEX at 0.6 ns at an axial position $z = 300 \mu\text{m}$, a radiative cooling time of $\tau_{\text{rad}} = 40 \pm 10$ ps was obtained. This very short radiative cooling time is consistent with the simulated temperatures on axis dropping by a factor of ~ 4 in 100 ps, and by an order of magnitude over 0.5 ns.

The present laboratory-produced jets can be described in terms of three-dimensionless quantities [2,3]: internal Mach number $M = v_{\text{jet}}/c_s$, where c_s is the sound speed within the jet, density contrast

$\eta = \rho_{\text{jet}}/\rho_{\text{ambient}}$; and the cooling parameter, $\chi = (\text{cooling length})/(\text{jet radius}) \approx v_{\text{jet}}\tau_{\text{rad}}/r_0$. Using the results from the jet simulations, values of $M \approx 15$, $\eta \gg 10^2$, and $\chi \approx 1$ were calculated, indicating a high Mach number, radiatively cooled jet. Simulations of typical astrophysical jets [2,3] give $M \approx 10$ –20, $\eta = 1$ –10, and $\chi \approx 0.1$ –10. Thus, the present laboratory-produced radiative jets are similar to astrophysical jets in Mach number and cooling parameter, but not well matched in density contrast. Future experiments will vary η to produce laboratory results more similar to their astrophysical analogs.

The authors thank D. Ryutov and N. Turner for theoretical support and S. Compton for technical assistance in conducting these experiments. This work was performed under the auspices of the U.S. Department of Energy by Lawrence Livermore National Laboratory under Contract No. W-7405-ENG-48. J.S. acknowledges the support of a Department of Energy High-Energy-Density Science grant.

-
- [1] S. Heathcote *et al.*, *Astron. J.* **112**, 1141 (1996).
 - [2] J.M. Blondin, B.A. Fryxell, and A. Konigl, *Astrophys. J.* **360**, 370 (1990).
 - [3] J.M. Stone and M.L. Norman, *Astrophys. J.* **413**, 198 (1993).
 - [4] M.L. Norman, L. Smarr, K.H.A. Winkler, and M.D. Smith, *Astron. Astrophys.* **113**, 285 (1982).
 - [5] R. Ouyed, R.E. Pudritz, and J.M. Stone, *Nature* (London) **385**, 409 (1997).
 - [6] J.M. Marti *et al.*, *Astrophys. J.* **479**, 151 (1997).
 - [7] L.M. Logory *et al.* (to be published); P.L. Miller, T.A. Peyser, P.E. Stry, and K.S. Budil, in *Shock Waves*, edited by B. Sturtevant, J. Shepard, and H. Hornung (World Scientific, River Edge, NJ, 1995), pp. 581–586.
 - [8] E.M. Campbell *et al.*, *Laser Part. Beams* **9**, 209 (1991).
 - [9] K.S. Budil *et al.*, *Rev. Sci. Instrum.* **67**, 485 (1996).
 - [10] P.M. Bell *et al.*, *Rev. Sci. Instrum.* **63**, 5073 (1992).
 - [11] S.G. Glendinning *et al.*, in *Applications of Laser Plasma Radiation II*, SPIE Proceedings Vol. 2523 (SPIE—International Society for Optical Engineering, Bellingham, WA, 1995), p. 29.
 - [12] H.F. Robey, K.S. Budil, and B.A. Remington, *Rev. Sci. Instrum.* **68**, 792 (1997).
 - [13] S.H. Glenzer *et al.*, *Phys. Rev. Lett.* **82**, 97 (1999).
 - [14] G.B. Zimmerman and W.L. Kruer, *Comments Plasma Phys. Control. Fusion* **2**, 51 (1975).
 - [15] M.K. Prasad, A.I. Shestakov, D.S. Kershaw, and G.B. Zimmerman, *J. Quant. Spectrosc. Radiat. Transfer* **40**, 29 (1988).
 - [16] W.A. Lokke and W.H. Grasberger, LLNL Internal Report No. UCRL-52276, 1977.
 - [17] D.L. Book, in *NRL Plasma Formulary* (Naval Research Laboratory, Washington, DC, 1987), p. 34.